Remote Sensing Applications: Society and Environment 29 (2023) 100891

Contents lists available at ScienceDirect

Remote Sensing Applications: Society and Environment

journal homepage: www.elsevier.com/locate/rsase

Monitoring Uruguay's freshwaters from space: An assessment of different satellite image processing schemes for chlorophyll-a estimation

J.M. Barreneche[a,*], B. Guigou[a], F. Gallego[a,b], A. Barbieri[a,c], B. Smith[d,e], M. Fernández[a], V. Fernández[a,c], N. Pahlevan[d,e]

[a] División Información Ambiental, Ministerio de Ambiente, Montevideo, 11100, Uruguay
[b] Instituto de Ecología y Ciencias Ambientales, Facultad de Ciencias, UdelaR, Montevideo, 11400, Uruguay
[c] Departamento de Geografía, Facultad de Ciencias, UdelaR. Montevideo, 11400, Uruguay
[d] NASA Goddard Space Flight Center, Greenbelt, MD, USA
[e] Science Systems and Applications, Inc. (SSAI), Lanham, MD, USA

ARTICLE INFO

Keywords:
Atmospheric correction
Chlorophyll-*a* algorithms
Landsat-8
Sentinel-2
Sentinel-3
Sustainable development goal 6
Water quality
Validation

ABSTRACT

Uruguay's freshwater network is threatened by widespread Harmful Algal Blooms (HABs) known to be triggered by human-related stressors such as land-use change and urban/industrial effluents. Existing field-based monitoring practices are limited due to their sparse spatial and temporal coverage. A complementary approach these techniques is to utilize remotely sensed observations for estimating optically relevant water-quality (WQ) parameters, of which chlorophyll-*a* (Chl*a*) is a robust proxy for HAB quantification. There is, however, a lack of information on apt country-scale image processing schemes, i.e., the best combination of Chl*a* algorithms, atmospheric correction (AC) methods, and satellite sensors that agree best with *in situ* Chl*a* across Uruguay's inland and coastal waters. Here, we analyze the accuracy of three different combinations of ACs (SeaDAS, POLYMER, and ACOLITE) and 17 Chl*a* models applied to the Operational Land Imager (OLI), Multispectral Instrument (MSI), and Ocean and Land Color Imager (OLCI) onboard Landsat 8, Sentinel-2A/B, Sentinel-3A/B, respectively. The performance of different processing schemes was assessed both in terms of their numerical consistency with *in situ* Chl*a* and classification accuracy for discriminating low vs. high Chl*a* with an 8 mg m^{-3} decision boundary. Our results show that the Mixture Density Networks (MDN) algorithm is often among the top performers. Other strong results were achieved by Gons (2 bands), Moses (3 bands) and Normalized Difference Chl*a* Index algorithms. Regarding the atmospheric correction processors, POLYMER works better for OLCI, and SeaDAS for the OLI, while no clear distinction among AC methods was found for MSI. Furthermore, the MDN model was also among the most reliable for assigning water pixels to low or high Chl*a* ranges. This could represent a key criterion for discriminating water bodies with good ambient conditions critical for reporting nationwide Sustainable Development Goal (SDG) 6.3.2 and other monitoring applications.

* Corresponding author.
E-mail address: jumanbar@gmail.com (J.M. Barreneche).

https://doi.org/10.1016/j.rsase.2022.100891
Received 20 August 2022; Received in revised form 16 November 2022; Accepted 25 November 2022
Available online 10 December 2022
2352-9385/© 2022 The Author(s). Published by Elsevier B.V. This is an open access article under the CC BY license (http://creativecommons.org/licenses/by/4.0/).

1. Introduction

Aquatic ecosystems are a vital component of human life, biodiversity, and biogeochemical regulations of the carbon cycle (Wetzel, 2001; Cole and Weihe, 2015). In recent decades, industrial developments, agricultural intensifications, and urban expansions have led to degradations in water quality, and, thus a decrease in key ecosystem services aquatic environments garnish (Board, 2005).

In 2015, the United Nations defined and addressed Sustainable Development Goal 6 (SDG 6), linked to clean water and urban sanitation (Connor, 2015). As part of this SDG target, two indicators were defined: a) SDG 6.3 to improve water quality (WQ) by reducing pollution, and eliminating /minimizing the release of hazardous chemicals and materials, and b) SDG 6.6 to protect and restore water-related ecosystems. In addition to this SDG target, another SDG indicator (SDG 14.1) that calls for preventing and significantly reducing marine pollution was specified. This SDG indicator is closely tied to the SDG 6 indicators and is relevant to WQ monitoring in freshwater-marine transition zones.

Effective monitoring of biophysical parameters specifying WQ conditions is paramount for understanding the dynamics of aquatic ecosystems and improving their management (World Health Organization, 2003). The traditional ground-based methods for measuring WQ parameters are costly, laborious, and insufficient due to their limited spatial and temporal coverage (El Serafy et al., 2021). The traditional WQ monitoring across Uruguay has been carried out by government agencies in inland and coastal waters since 2004, and covers a diverse range of biological and physicochemical parameters (e.g., total nitrogen, dissolved oxygen, thermotolerant coliforms) (Ministerio de Ambiente [MA], 2021).

The impacts of land-use change and urban/industrial effluents on drinking water supplies and recreational waters of Uruguay have been well recorded for at least a decade (Aubriot et al., 2017; Gorgoglione et al., 2020). Over the last three decades, a major rise in anthropogenic pressure associated mainly with land-use change (afforestation and croplands) and industrial/urban effluents has significantly deteriorated WQ nationwide. More recently, degradations in WQ have been caused by Harmful Algal Bloom (HAB) events that have irrevocable economic implications through the loss of tourism and increased treatment costs. Due to this mounting pressure, field monitoring techniques cannot capture the high spatiotemporal variability of HABs; therefore, complementary measurement methods such as those offered through remote sensing must be harnessed.

Remotely sensed radiometric observations can estimate optically relevant WQ parameters, such as near-surface concentration of chlorophyll-*a* (Chl*a*) or total suspended solids (TSS), for which a considerable and growing number of algorithms have been developed (see comprehensive lists in Neil et al., 2019; Pahlevan et al., 2020; Balasubramanian et al., 2020). In recent years, this approach has seen an increase in its application and is currently being incorporated as an optional measurement technique in the SDG 6.3.2 methodological guide, specifically in Level 2 reporting (Andries et al., 2019; Ferreira et al., 2020).

The primary advantage of remote sensing data is the improved spatial and temporal coverage compared to traditional field-based monitoring exercises. Although satellite data processing methods continue to mature, the use of satellite information for augmenting sparse ground-based monitoring approaches enhances the spatial extent and the revisit frequency of a waterbody of interest (Palmer et al., 2015; Moses et al., 2017).

Prior to the beginning of the millennium, NASA's advancements in developing ocean-color missions (Gordon et al., 1983) and its open data policy led to major algorithm developments (O'Reilly and Werdell, 2019). Similar Chl*a* algorithms (e.g., band ratio methods) suited for optically complex waters were also conceptualized and implemented in the 1990s (Gitelson, 1992; Bukata et al., 1995), but did not become operationalized until toward the end of the Medium Resolution Imaging Spectrometer (MERIS) mission lifetime (Moses et al., 2012) when the imagery was released publicly (Palmer et al., 2015). Fueled by the availability of high-resolution sensors, such as OLI (Operational Land Imager; 30 m), MSI (MultiSpectral Instrument; 10 m), and OLCI (Ocean Land Color Instrument; 300 m), together with more support for field campaigns involving optical measurements (Gernez et al., 2017; Poddar et al., 2019), the rate in the emergence of novel algorithms has significantly risen in recent years. Yet, few investigations have analyzed the accuracy of downstream Chl*a* products, warranting further assessments of the effects of uncertainties from atmospheric correction (AC). Pahlevan et al. (2020) carried out a global analysis comparing different models and ACs while also proposing a novel algorithm, termed Mixture Density Networks (MDNs), for the estimation of Chl*a* in coastal and inland waters. However, the performance of different algorithms in conjunction with AC processors has not been widely assessed at national or regional scales.

Uruguay has limited research activities surrounding satellite-based WQ retrievals and monitoring. For instance, no efforts have been dedicated to assessing the performances of a suite of retrieval algorithms and AC methods for a wide range of water bodies throughout the country. Research of this kind is focused on a few regions, with an evaluation of global and local algorithms using field measurements, and the effectiveness of different ACs for local water bodies has not been studied (Drozd et al., 2020; Maciel and Pedocchi, 2021; Zabaleta et al., 2021;).

The objective of this work is to analyze the accuracy of a select combination of three sensors, three AC methods, and seventeen Chl*a* estimation models, i.e., processing schemes, to identify best-practice algorithms for Chl*a* estimation in nine water bodies of Uruguay's inland and coastal systems. Furthermore, we assessed the performances of these schemes when working with two rudimentary classes of water, defined by a cutoff value for field sampled Chl*a*, and also evaluated their success in assigning the correct water class for each sample. In the Methods (section 2), we provide a brief description of the area of study and the techniques by which field and satellite data were obtained, followed by the definitions of the metrics used for performance evaluation. Metrics are presented in separate subsections: one for the regression metrics and two for the global metrics used to aggregate the results: Mean Normalized Ranking (MNR) and Youden's J statistic. In the Results (section 3), we present the satellite matchups and assessments of different schemes in terms of both their global performance and binary (high vs. low Chl*a*) classification capability. We then explored the implications of our findings for scientific studies and monitoring applications, in sections 4 and 5, Discussion and Conclusions, respectively.

2. Methods

2.1. Study area

This study was carried out across continental and coastal water bodies of Uruguay, including rivers, reservoirs, lagoons, and coastal areas (Fig. 1). Different anthropogenic interventions, such as urban and industrial activities, croplands, and tourism, affect these ecosystems.

The Río Negro is the most important inland watercourse in Uruguay and has three hydroelectric generation reservoirs, Palmar, Baygorria, and Rincón del Bonete, that affect the main channel flow regime. Its basin area, 70.7 km^2, occupies around 38% of Uruguayan territory. Its waters are used mainly for irrigation and tourism, while the basin's predominant land-use includes croplands, afforestation, and grasslands associated with livestock.

The Río de la Plata, an estuarine system formed from the discharge of the Paraná and Uruguay rivers and the second largest basin of the continent. The main economic activities of the basin are associated with agricultural production and industry.

Three lagoons are also included in the monitoring sites: "del Sauce", "José Ignacio" and "Garzón". The Sauce Lagoon supplies more than 95% of the fixed and floating population of the Maldonado department. The two main activities in its basin are croplands and afforestation. José Ignacio and Garzón lagoons are coastal water bodies that periodically connect with the Atlantic Ocean through natural and artificial openings (Rodríguez-Gallego et al., 2003).

A single site on the Cuareim River, a tributary of the Uruguay River and the border between Uruguay and Brazil, was also included The river basin (8.2 km^2) includes various human activities such as livestock, rice, sugar-cane plantations, and mining activity (semi-precious stones).

2.2. In situ Chla data

In situ Chl*a* data were gathered during several WQ monitoring campaigns carried out by the Ministry of the Environment of Uruguay. Monitoring stations are indicated in Fig. 1. These data contributes to a database of >3000 Chl*a* samples, spanning the 2004–2020 period. The data collection in the field follows the Global Environmental Monitoring System (GEMS) Water Operational Guide (Allard and World Health Organization, 1992) , and the laboratory analysis was performed following the guidelines of the Ministry of the Environment, which is subject to the ISO 9001 quality management system (Ministerio de Vivienda, Ordenamiento Territorial y Medio Ambiente [MVOTMA], 2017). The reference analytical methodology for Chl*a* analysis is the U.S. Environmental Protection Agency (EPA) method 446.0, which explains in vitro determination of Chl*a* and phaeopigment via visible spectrophotometry.

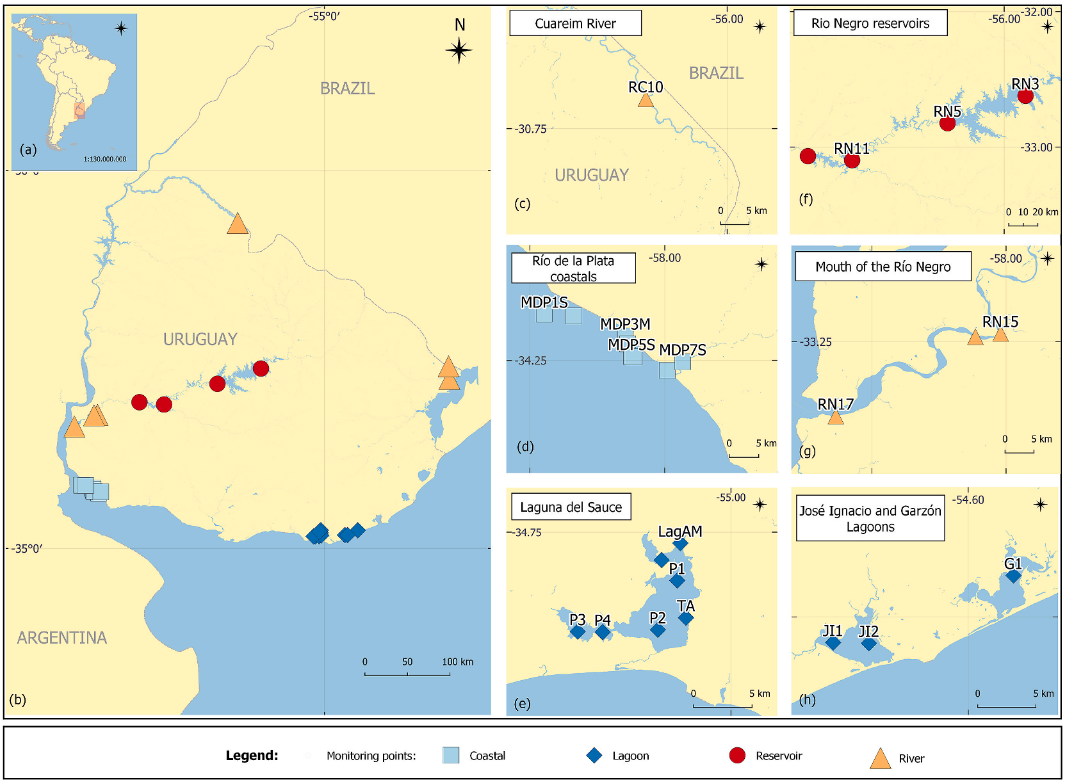

Fig. 1. Geographic distribution of field monitoring sites. a) Uruguay in South America, b) location of monitoring sites according to the type of water body, c) Cuareim River, d) Río de la Plata coast, e) Laguna del Sauce, f) Rio Negro reservoirs, g) Mouth of the Río Negro, and h) José Ignacio and Garzón Lagoons.

2.3. Satellite images, atmospheric corrections, and matchups

For this study, OLI (Landsat 8), MSI (Sentinel 2), and OLCI (Sentinel 3) imagery were evaluated for monitoring Chl*a* as a proxy for analyzing the trophic state. Information about the sensor characteristics is provided in Table 1.

A range of AC methods is available to process satellite products, each with merits based on the target applications and scientific objectives. For example, Pahlevan et al. (2021) showed that ACOLITE, POLYMER, and SeaDAS can produce meritorious aquatic reflectance products over inland and coastal waters with varying degrees of success across different optical water types. These processors have also been utilized and suggested in other research endeavors (Mograne et al., 2019; Pahlevan et al., 2019; Warren et al., 2019), warranting their utility in this study. While other applicable AC processors (Pahlevan et al., 2021) may still be viable, in this study, we assess these three AC processors.

ACOLITE (version 20190326.0) applies a dark spectrum fitting, assuming a homogeneous atmosphere in pixels with R_{rs} very close to zero (Vanhellemont, 2019). In this study, ACOLITE was only utilized to correct OLI and MSI imagery. POLYMER (version 4.11; Steinmetz et al., 2011) finds the best fit of R_{rs} for a TOA reflectance and a collection of models of aerosols, scattering, and brightness signals. This correction shows optimal results in areas affected by flare or adjacency effects (Bulgarelli et al., 2014). SeaDAS generates R_{rs} by removing the aerosol from the Rayleigh corrected spectra in the visible spectrum bands using the information the NIR and/or short-wave infrared band ratios. Here, we applied the band combinations 865–1613 nm for MSI (Pahlevan et al., 2017), 865–1609 nm for OLI, and 779–865 nm for OLCI (SeaDAS v7.5). Additionally, pixels that did not pass through the standard Level 2 flags, i.e., ground, high/saturated glow, stray light, and cloud/ice, were excluded from the analysis.

Satellite-derived Chl*a* matchups were obtained by selecting pixels that matched the times and locations of *in situ* Chl*a* samples. To maximize the number of matchups, particularly in nearshore waters, only single pixels containing the exact coordinates of the *in situ* samples were considered. For the same reason, temporal misalignments of up to 5 h, from 9 a.m. to 5 p.m. local time, were accepted. Sample locations too close to shorelines and man-made objects or pixels contaminated with residual clouds, cloud shadows or sunglint were excluded.

Preliminary analyses showed that many algorithms produced extreme values of Chl*a* for some matchups. Most of these were explained by unusually low values in one or more satellite band reflectances, e.g., when the reflectance quotient between the blue and green bands is lower than 0.1, estimations for the algorithm OC2 (Ocean Color for 2 bands), reaches values above 8 million mg m^{-3} for Chl*a* (O'Reilly and Werdell, 2019). Most extreme values were produced by algorithms that use a variation of the quotient between band reflectances as the main input. These are cases outside the reflectance ranges for which they were trained. To avoid biased analyses due to these predictions, values greater than 100,000 mg m^{-3} were removed. For similar reasons, following Morley et al. (2018), low *in situ* and satellite-derived Chl*a* values were modified so that they at least matched the lowest quantitation limit reported in the original database, 0.1 mg m^{-3}. Across satellite and AC methods, the *in situ* Chl*a* for matchups were not evenly distributed, with MSI having the largest number of matchups (Fig. 2). The discrepancy in the number of matchups among processors for a single sensor is caused by the differing cloud-masking approaches applied by each processor (supplementary material, Table S2).

The outputs of AC processors were used as input for Chl*a* models. Throughout this article, we use the term scheme to refer to a particular combination of satellite sensors, AC, and Chl*a* algorithms (Table 2). In total, 88 schemes (42 for MSI, 34 for OLCI, and 12 for OLI) were evaluated and ranked using several performance metrics.

2.4. Chlorophyll-a retrieval algorithms

The performance of Chl*a* retrieval algorithms was assessed by comparing the measured *in situ* concentrations against the satellite-retrieved Chl*a* for 17 algorithms. The analysis includes global (e.g., Pahlevan et al., 2020) and local algorithms (Drozd et al., 2020) (Table 2).

Model performances were evaluated twice: firstly, for the whole dataset, and secondly, for two partitions (high and low *in situ* Chl*a*). Range-based analyses of algorithms can help identify specific algorithms for individual ecosystems across Uruguay, and algorithms are expected to perform differently for various ranges of Chl*a* (Pahlevan et al., 2020, 2021), as they may fall inside or outside the ranges for which they were trained (Table 2). Due to the limited availability of matchups at higher concentrations (Fig. 2), a single cutoff value of 8 mg m^{-3} was adopted, dividing the dataset into two classes. This value was selected after the classification proposed by the Organization for Economic and Co-operative Development (OECD), which is used in government documents (MA, 2021;

Table 1
Sensor characteristics.

	Operational Land Imager (OLI)	MultiSpectral Instrument (MSI)	Ocean Colour Land Instrument (OLCI)
Nominal spatial resolution (m)	30	10, 20, 60	300
Swath width (km)	185	290	1270
Useable Spectral bands (nm) for Chl*a*	443, 482, 560, 655	443, 492, 560, 665, 705, 740, 783	410, 443, 490, 510, 560,620, 665, 673, 681, 708, 753, 778
Average overpass time (UTC) over Uruguay	13:35	13:50	13:00
Lifespan	2013 – to present	2015 – to present	2016 – to present
Source	https://earthexplorer.usgs.gov	https://scihub.copernicus.eu	

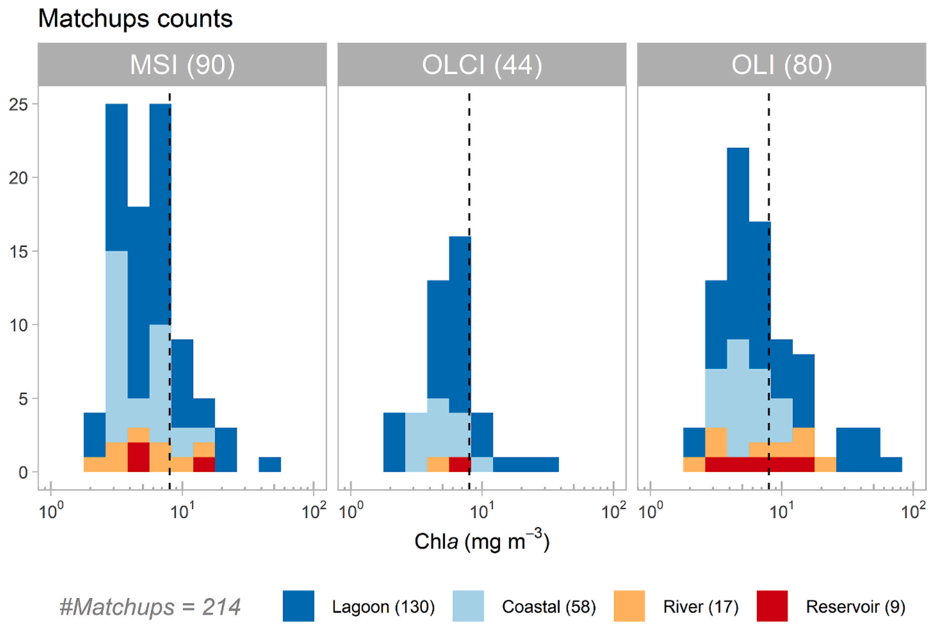

Fig. 2. Distribution of valid matchups across sensors and water bodies. The vertical dashed line indicates 8 mg m^{-3}. Legend colors correspond to those shown in Fig. 1. The total number of matchups is 214; matchups for Chl*a* below and over 8 mg m^{-3} are included in Table S5 of the supplementary material.

Table 2
List of analyzed models and the corresponding bibliographic references. The last column includes the range of Chl*a* values for which each model was trained.

Model	Reference	Chl*a* Range (mg m^{-3})
Drozd	Drozd et al., 2020	4–4700
Gilerson (2 bands)	Gilerson et al. (2010)	<221
Gilerson (3 bands)	Gilerson et al. (2010)	<221
Gons (2 bands)	Gons (1999)	3–185
Gurlin (2 bands)	Gurlin et al. (2011)	0–100
Gurlin (3 bands)	Gurlin et al. (2011)	0–100
MDN	Pahlevan et al. (2020)	<150
Mishra NDCI	Mishra & Mishra (2012)	<30
Moses (2 bands)	Moses et al. (2009)	10–40
Moses (3 bands)	Moses et al. (2009)	10–40
OC2	O'Reilly & Werdell (2019)	<78
OC3	O'Reilly & Werdell (2019)	<78
OC4	O'Reilly & Werdell (2019)	<78
OC5	O'Reilly & Werdell (2019)	<78
OC6	O'Reilly & Werdell (2019)	<78
Smith Blend	Smith et al. (2018)	<221
Yang Bandindex	Yang et al. (2011)	<140

OECD, 1982), and defines five classes with cut-off points at 2.5, 8, 25, and 75 mg m^{-3} of Chl*a*. This value is used as a threshold between oligotrophic and mesotrophic waters in official publications (MA, 2021).

Model predictions were also evaluated regarding their ability to classify waters into low or high Chl*a* samples, as determined by the cutoff of 8 mg m-3. For this binary classification, a different set of performance metrics was used.

2.5. Performance evaluations

2.5.1. Regression metrics

A set of metrics was selected to evaluate each scheme. In particular, complementarity is necessary to avoid biases inherent to different metrics. Considering this aspect and the characteristics of the dataset, five metrics were selected, *MSA*, ε, β, *I,* and *S*, which are defined as follows:

$$MSA\ (\%) = 100 \times \left(10^X - 1\right) \quad \text{where}\ \ X = \frac{1}{n}\sum_{i=1}^{n}\left|\log_{10}\left(E_i/M_i\right)\right| \tag{1}$$

$$\varepsilon\ (\%) = 100 \times \left(10^{Y} - 1\right) \quad \text{where } Y = Median\ \left(\left|\log_{10}(E/M)\right|\right) \tag{2}$$

$$\beta\ (\%) = 100 \times sign(Z) \times \left(10^{|Z|} - 1\right) \quad \text{where } Z = Median\ \left(\log_{10}(E/M)\right) \tag{3}$$

$$\log_{10}\left(E_i\right) = I + \log_{10}\left(M_i\right) \times S \tag{4}$$

Where E and M (mg m^{-3}) refer to values of Chl*a* estimated by predictive models and measurements taken *in situ*, respectively; i is the index that indicates the ith value of the set of observations and n is the total number of observations. Equation (4) describes the line formula used to obtain S and I, the Slope and Intercept, which were computed with the non-parametric Theil-Sen linear regression technique.

The first three metrics, MSA, ε, and β (Mean Symmetric Accuracy; Median Symmetric Accuracy; Symmetric Signed Percentage Bias; Morley et al., 2018), are based on the logarithm of E/M and should be read as the percentage increase of E relative to M. These are robust metrics that are suited for variables with heavy-tailed distributions, like Chl*a* (Morley et al., 2018). Nevertheless, they also reward cases where variability is low, with most predicted (E) values around the average field measurement (M), regardless of how close the points fall to the 1:1 line in E vs. M space. Such cases can occur frequently when a fewer number of matchups and/or range of *in situ* Chl*a* are available for any given scheme. Both I and S were added to the list of metrics to counterbalance this tendency. In a similar vein, MSA is included for its use of the average function instead of the median. This adds penalization to cases with higher noise.

2.5.2. Mean Normalized Ranking

To choose the best-performing schemes, the Mean Normalized Ranking (MNR), was developed. This ranking technique rewards consistency across different metrics and a more holistic evaluation of schemes. The calculation of MNR involves two steps: ranking all schemes according to individual metrics and then normalizing and averaging the scores across all metrics for each. The values obtained for MNR can be used as an approximate selection, which should be complemented by closer examination of individual cases. It does not provide an absolute measure of performance, which is what individual metrics do, but aids in selecting the best case, given a set of options. The calculation of MNR is described thusly:

$$MNR\ (\%) = 100 \times \frac{1}{N} \sum_{m=1}^{N} r'_m \quad \text{where } r'_m = \frac{r_m}{C} \tag{5}$$

N is the number of metrics evaluated, C is the number of schemes, and r_m is the position of an individual scheme on the ranking obtained by metric m. To determine r_m, the schemes are ranked according to the values obtained for the metric m, in descending order (i.e.: $r_m = 1$ or $r_m = C$, for worst and best performances, respectively), using the maximum for resolving ties. These rankings must take into account the different criteria for numeric performance that different metrics may have (e.g., zero is the optimal value for MSA, but not for S). Absolute values of deviations from optima were used to assess all r_m.

2.5.3. Classification metrics

Binary classification problems are concerned with assigning observations to one of two categories: positive or negative. Hence, all predictions fall into True Positives (TP), True Negatives (TN), False Positives (FP), and False Negatives (FN); the latter two are also known as Type I and II errors. Many metrics can be drawn from these values to gauge performance. Two competing and frequently used are Sensitivity and Specificity:

$$\text{Sensitivity} = \text{TP} / (\text{TP} + \text{FN})$$

$$\text{Specificity} = \text{TN} / (\text{TN} + \text{FP})$$

Sensitivity is the proportion of Positives that are correctly predicted as such (Chl*a* $\geq$ 8 mg m^{-3}), and Specificity is the proportion of Negatives (Chl*a* $<$ 8 mg m^{-3}) that are correctly classified. Both fall in the [0, 1] range. An ideal scheme would score 1 on both metrics, while overly biased ones would favor one over the other (i.e., overestimating Positives or Negatives). To rank the results, Youden's J statistic was used (Youden, 1950):

$$\text{J} = \text{Sensitivity} + \text{Specificity} - 1$$

All the statistical analyses in this article were done using R software (R Core Team, 2018), including the package RobustLinearReg (Hurtado, 2020) for performing Theil-Sen linear regressions.

3. Results

3.1. Matchups

A sum of 992 Chl*a* estimates (~22% of our database) was discarded after applying all the filters (Section 2.3), and 21 Chl*a* algorithm predictions lower than 0.1 mg m-3 were modified to 0.1 mg m^{-3}. In total, 194 *in situ* samples, amounting to 214 matchups, were used (note that a single field sample can match-up with more than one satellite pass). Matchup dates ranged between 2013 and

2020, with the number of matchups per year varying from 6 (2015) to 46 (2017 and 2018), and an average of 26.75 yearly matchups. From all the algorithms (Table 2), 3477 Chl*a* estimations were evaluated (Table S1).

3.2. Performance analysis

In terms of MNR, models generally exhibit a wide range of performance, suggesting a considerable influence of the AC method for the three sensors and various schemes (Fig. 3). Moreover, the set of matchups used to evaluate a particular scheme is can differ from the next, which can make intercomparisons difficult. Scores for MSI schemes were highly variable, with no clear bias for any AC. On the other hand, OLCI images, processed only with POLYMER and SeaDAS, had marked and consistent differences between AC, with better results for POLYMER (Fig. 3). When considering the median MNR for each model, the top three performances were Mishra, Gons (2 bands) and MDN. Although the MDN is ranked in third place, it is the only one that can be applied to all three sensors and exhibits the best individual results per sensor: MSI-ACOLITE, OLCI-POLYMER, and OLI-ACOLITE (Fig. 3; Figs. 4–6; Table S3). Other models, such as Moses (3 Bands), OC2, and OC3, also scored highly on specific combinations of sensor and AC (Fig. 3).

While MDN has the highest scores across all sensors, for the OLCI cases the results are not far from Gons and Moses (3 Bands) algorithms (Fig. 5, S6). On the other hand, within the universe of combinations of MSI-ACOLITE, MDN achieved much stronger results, reflected in a difference >14% in MNR with the second best algorithm (Fig. 4). Regarding OLI, results seem unable to reproduce the dynamic range of the *in situ* Chl*a* data, as most of the slopes obtained were close to zero (with ACOLITE-MDN and SeaDAS-OCx, as possible exceptions; Fig. 6). A complete set of scatter plots is provided in the supplementary material (Figures S3 to S10).

Most schemes tend to overestimate Chl*a*, as shown by the positive bias of β values (Figs. 4–6; Fig. S1). Regarding *I* and *S*, most models were skewed over and under the expected results: around 1 for *I*, and 0 for *S* (Figs. 4–6; Fig. S2). An *I* of 1 would mean E = 9 mg m^{-3} at M = 0, and an *S* of 0 implies a constant prediction for the whole range (Eq. (5)). This pattern suggests that these schemes predict near-constant values that are close to the mean M (~ 8.01 mg m^{-3}). Most OLI schemes (Fig. 6; Figs. S8-S10) and the schemes that combine OLCI and SeaDAS (Fig. 5; Fig. S7) fall strongly into this category. Interestingly, some of the formers scored above-average MNR values, such as OLI-MDN or OLI-OCx-SeaDAS (Fig. 3). Among other cases exhibiting similar patterns, many OLCI schemes stand out. These scenarios were evaluated over the lowest number of matchups (between 20 and 34), so a few bad predictions could skew the linear model fit, but no specific source of error was identified. More generally, the pattern of constant Chl*a* predictions suggests a low capacity of schemes for capturing the variability across these water bodies.

3.3. Water classes: high and low Chla concentrations

While MNR scores for low Chl*a* waters almost mirror the global results, the dispersion is much higher at greater concentrations (Fig. 3), which might be related to the matchup size (n) (49 vs. 145; Figs. 2 and 3; Table S5). At higher Chl*a* ranges, performances of MSI schemes fall consistently, including top performers (NDCI, Gons, and MDN), while many OLCI and OLI schemes achieve much better results. Whether the regression line (Eq. (4)) crosses the E = M line at lower or higher ranges (Fig. 6) is generally attributed to the performance for each water class (high MNR for low Chl*a*; MDN with ACOLITE or POLYMER; high MNR for high Chl*a*: POLYMER

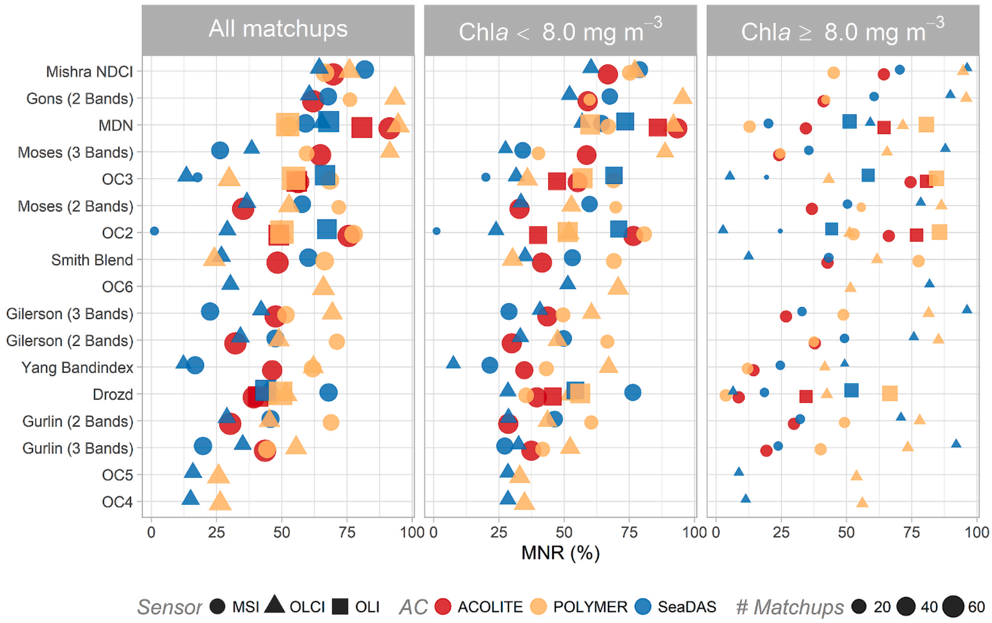

Fig. 3. MNR values across schemes for all valid (left) low Chl*a* (<8 mg m^{-3}; center), and high Chl*a* (≥8 mg m^{-3}; right) matchups. Models are ordered by their median MNR, obtained with all matchups. Each scheme (i.e., a combination of AC, retrieval algorithm, and sensor) is represented by a different shape and color-coded differently. The size is proportional to the number of matchups.

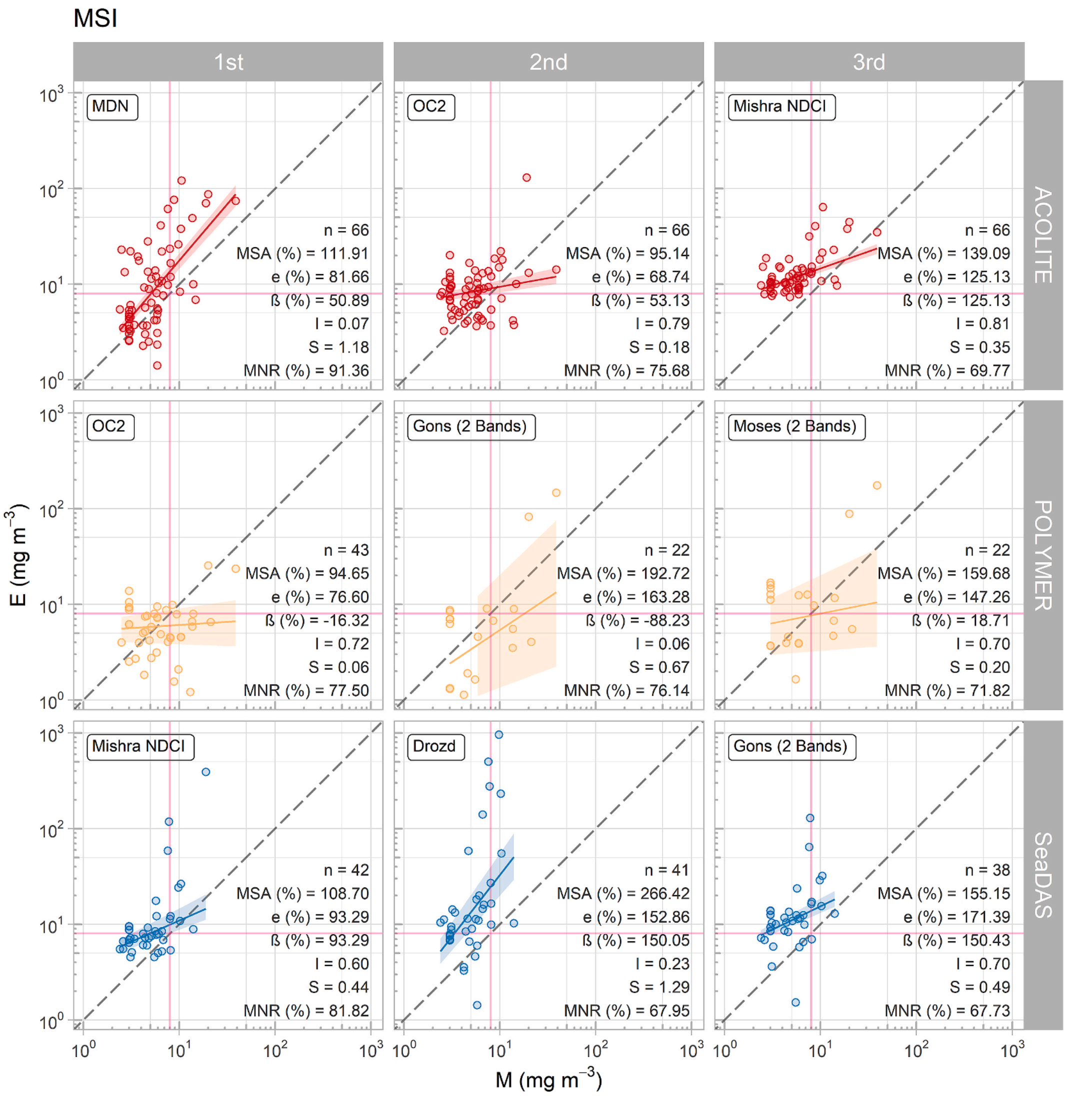

Fig. 4. Chl*a* estimations (E) versus *in situ* measurements (M) for MSI schemes, showing the top three algorithms (left to right; columns) according to MNR for all atmospheric corrections (rows). Vertical and horizontal magenta lines indicate the cutoff point of 8 mg m^{-3}.

schemes; OCx-ACOLITE). Regardless of all these considerations, several cases remain consistent in most or all trophic levels, such as OLCI-POLYMER-(Gons, NDCI, MDN, Moses 3 Bands), MSI-ACOLITE-OCx and MSI-POLYMER-Smith Blend.

3.4. *Classification (Youden's J statistic)*

Following the general overestimation of Chl*a*, most schemes scored highly in Sensitivity but low on Specificity (i.e., success in identifying highly eutrophic waters, but failure in properly recognizing low concentrations; Fig. 7; Table S6). In other words, type I errors (False Positives) were more common than type II errors (False Negatives). Some OLI schemes were close to the extreme in these cases, as they produce constant values around the average, which in most cases fell over the cutoff point of 8 mg m^{-3}, predicting most matchups to be positive (either TP or FP). On the other hand, top MNR performers were among the best achievers according to Youden's J metric (except for OLI-ACOLITE-MDN), even in cases where the MNR scores for high Chl*a* waters were low.

4. Discussion

This study sought to identify optimal processing schemes to enable practical satellite monitoring of Chl*a* across Uruguay's inland and coastal waters. We compared a broad spectrum of schemes that combine different predictive models for Chl*a* estimation with three satellite sensors and three atmospheric corrections. To streamline the comparative analyses where a large combination of models, ACs, and satellite sensors were involved, two global complementary metrics were used. In particular, the development of the novel statistic, the MNR, facilitated the comparison of the schemes in relative terms. The use of the Youden's J statistic aided in the

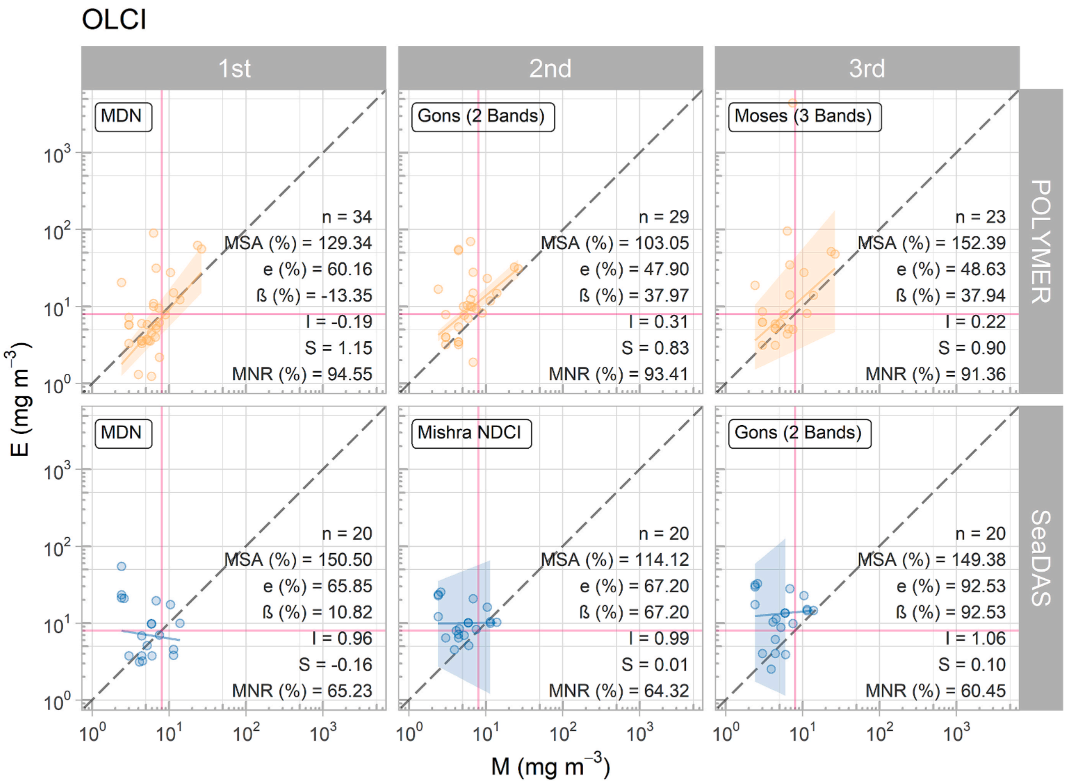

Fig. 5. Same as Fig. 4 only for OLCI processed via POLYMER and SeaDAS. The poor performances on the bottom row are common across OLCI-SeaDAS schemes (Fig. S7).

evaluation of the schemes in their ability to differentiate discrete categories of waters with high (meso-eutrophic) and low (oligo-mesotrophic) Chl*a*, which may not be evident through other metrics and can be crucial from a management perspective.

After inspecting performers in Figs. 4–6, it is useful to distinguish between two groups of schemes: those in which the regression lines have slopes around or higher than 1 (high-*S*) and those with Slopes below 1 (low-*S*). Several MSI and OLCI schemes are found in the first group, mostly paired with ACOLITE or POLYMER, while the second group includes most OLI and SeaDAS schemes, but also some MSI cases with ACOLITE and POLYMER (MSI results probably being the highest in disparity).

Most highly ranked combinations (MNR >80%) are among the high-*S* group, reflecting the weight of *S* and *I* in evaluating performance. These included the MSI-ACOLITE-MDN, OLCI-POLYMER-MDN, OLCI-POLYMER-Gons, and OLCI-POLYMER-Moses (3 Bands) schemes. The strongest aspect of these results is their ability to classify Chl*a* correctly, although they still suffer from estimation errors of around an order of magnitude in the most flagrant cases, even in the low ranges of *in situ* Chl*a*. In this regard, MSI-ACOLITE-MDN is the most notable, with a clear bias towards overestimation of Chl*a* across the range, although maybe more so on high Chl*a* ranges (Fig. 4).

Two schemes in the low-*S* group achieved MNR above 80%: MSI-SeaDAS-Mishra and OLI-ACOLITE-MDN, but only the former achieved high values of Youden's J statistic. These high performances could be associated with their lesser sensitivity to uncertainties induced by the AC in the red and NIR bands and also because a large portion of our samples was within their range of applicability (Mishra and Mishra, 2012). Nevertheless, the MSI-SeaDAS-Mishra scheme still underestimates Chl*a*, particularly at lower ranges, while also producing overestimated, or even extreme, values at higher ranges (Fig. 4). On the other hand, OLI-ACOLITE-MDN, as with most OLI combinations, seems to poorly capture changes in Chl*a* seen in the dataset, which is especially pronounced when inspecting the classification metrics (Fig. 7; Table S6). In this case, the high MNR score is explained mostly by MSA, ε, and β, which are generally better than that in other schemes.

Most high MNR scoring schemes in the high-*S* group also achieved high classification performance as seen in the Sensitivity, Specificity, and J scores. This can partially be traced to the regression lines being close to the 1:1 line around M = 8 mg m^{-3} (the cutoff value; see Figs. 4–7; Table S6). This not only applies to top-performing OLCI-POLYMER schemes, combined with MDN, Gons and Moses (3 Bands), but also for some low-*S* schemes, such as MSI-SeaDAS-Mishra. Among these high MNR and high-*S* schemes, the MSI-ACOLITE-MDN results are the most biased towards False Positives. Nevertheless, in terms of monitoring, sometimes a bias towards False Positives can be a preferable outcome, since it is generally in the public's interest to detect most or all HABs, particularly when resources are relatively limited.

Several instances of the MDN were among the top performers in terms of MNR and J statistic, suggesting robustness, although with disparity along schemes, as shown when comparing low and high *in situ* Chl*a* ranges (Fig. 3). Nonetheless, MDN achieved the top

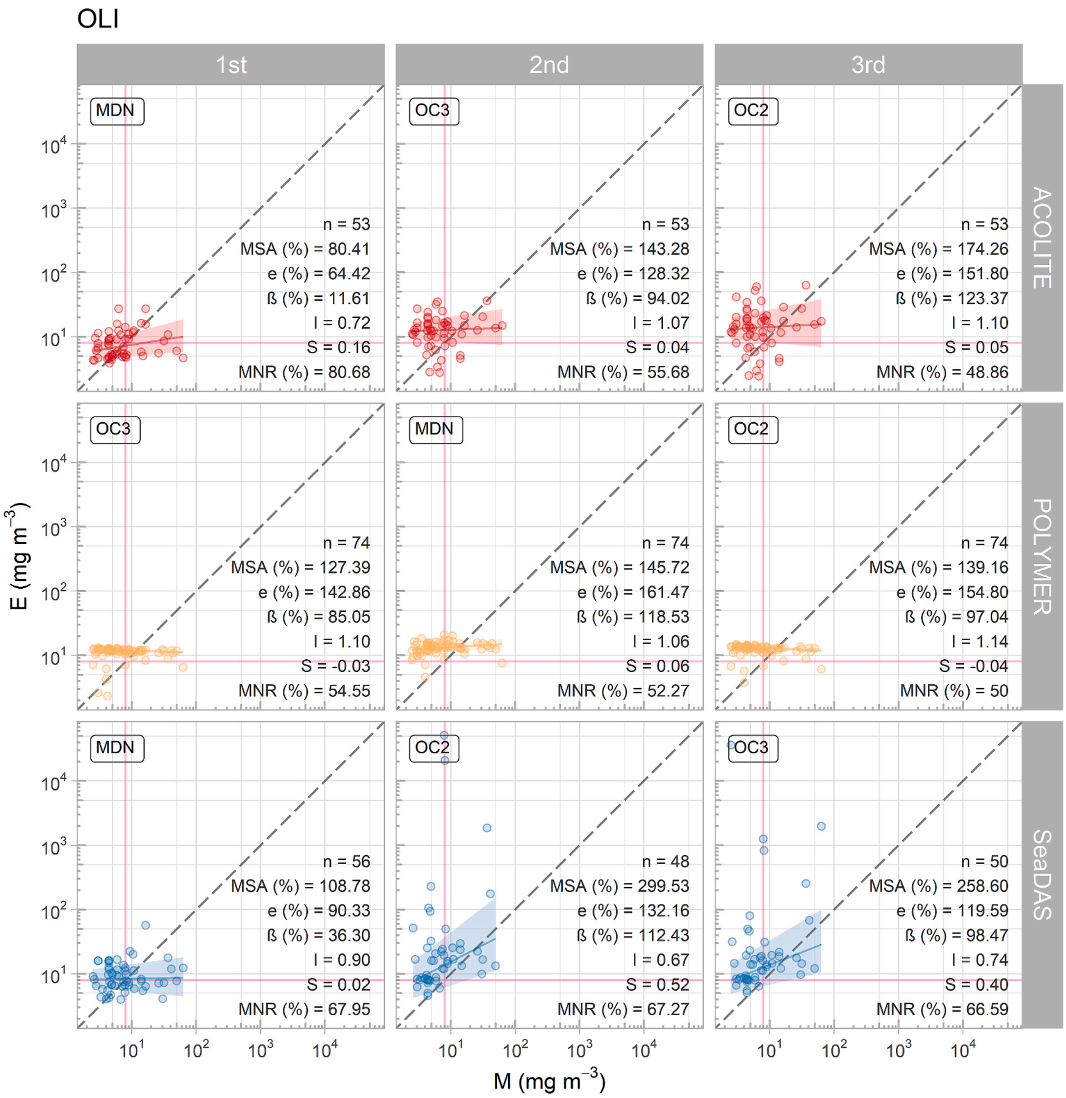

Fig. 6. Same as Figures 4 and 5. Axes are equal in range and were extended to include all data points, which can obscure the fact that the range of *in situ* values is the widest for all sensors (Fig. 4–6; Table S2).

performance for all sensors: OLCI-POLYMER, MSI-ACOLITE, and OLI-ACOLITE, with the former being the highest MNR score of the whole set. Both OLCI and MSI schemes may be adequate for satisfactory monitoring applications since they can detect important changes in concentration while mostly avoiding the frequent overestimation, seen across most algorithms. Nevertheless, a review of the causes for high Chl*a* estimates is warranted, including a closer examination of the behavior of ACs in Uruguayan waters.

Regarding the AC processors, our results suggest that POLYMER performs better for the OLCI sensor (particularly with MDN and Gons 2 bands). This may be associated with the use of more spectral bands (compared to MSI and OLI) in the optimization process built into POLYMER. For schemes where SeaDAS is applied, above-average results were obtained for NDCI, MDN, and Gons (2 bands), perhaps because of significant uncertainties in the blue bands in other models. We also observed acceptable results for low Chl*a* matchups for OLI, although care must be exercised when estimating Chl*a* from OLI. Other schemes appear to be generally among the worst performers, especially for the OLCI-OCx combination, though the small number of samples and low Chl*a* values may skew our results. This is likely due to the use of two NIR bands for approximating aerosol contributions over highly scattering waters which can lead to inaccurate R_{rs} estimates (Mélin et al., 2011). Finally, ACOLITE yields intermediate results, showing the best results in combination with the MDN model for both OLI and MSI. Other AC processors adept at handling atmospheric effects in inland waters, such as the image CORrection for atmospheric effects (iCOR; De Keukelaere et al., 2018), may prove viable in Uruguay freshwaters, in particular, in nearshore regions where adjacency effects may be present. The other suitable processor is the Glint Removal for Sentinel-2 (GRS; Harmel et al., 2018), which accounts for MSI pixels impacted by sunglint. The Case-2 Extreme Waters (C2X) has also exhibited reasonable performances for OLI, MSI, and OLCI (Renosh et al., 2020). Overall, recognizing AC as one primary source of uncertainty

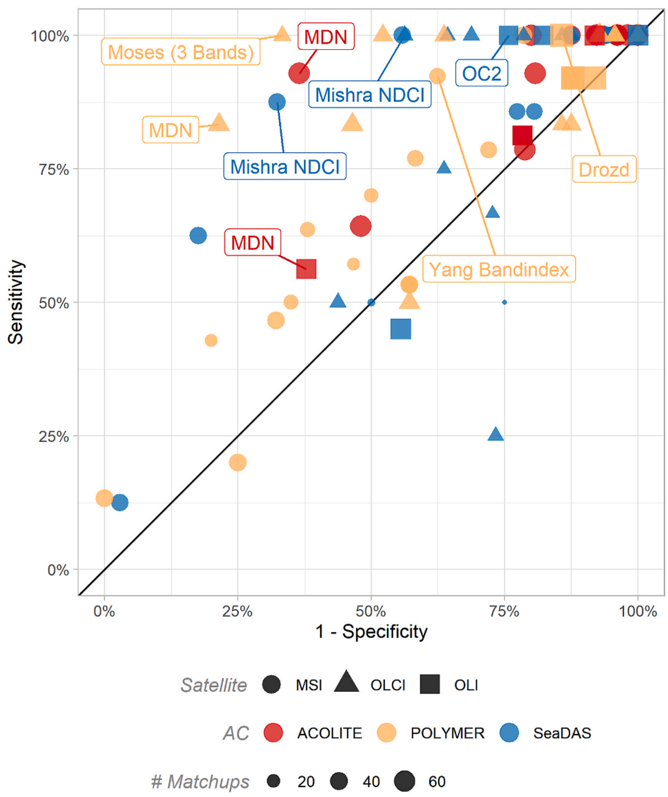

Fig. 7. Sensitivity and 1 - Specificity metrics of all possible schemes indicating a correct prediction of high and low Chl*a*, respectively. The best results are those closer to the upper left corner. Named algorithms indicate the best global results for each processing scheme (supplementary material, Table S6).

in the total uncertainty budget of satellite-derived Chl*a* products, we anticipate the existing AC processors to evolve and new techniques to emerge, warranting the revision of our data processing workflow in the future.

A spatiotemporal examination of Chl*a* generated from the MSI-ACOLITE-MDN scheme over Rincón del Bonete reservoir is shown in Fig. 8. These images were acquired in the summer of 2021–2022 (December 11th, 2021, to March 31st, 2022) under clear sky conditions. This processing scheme shows the spatiotemporal dynamics of Chl*a* in the reservoir, when the entire water body was affected by HAB events characterized by Chl*a* $>$ 100 mg m^{-3} (e.g., Feb 9th, 2022). As the summer season begins, some moderate blooms are highlighted with high concentrations in the upstream portions of the reservoir, both in the main channel (Area 1, Fig. 8), as well as in the secondary branches (Areas 2 and 3, Fig. 8). From December to January, blooms become increasingly common, generally affecting specific areas, such as the branches (Areas 2 and 3, Fig. 8). Finally, blooms spread across the entire reservoir in February, with peak Chl*a* over vast areas of the water surface. Towards the end of the season, in March, enhanced Chl*a* become the norm, but extreme values ($>$100 mg m^{-3}) tend to shrink in extent and frequency. From a qualitative perspective, this map series closely agrees with the expected and reported behavior of HABs in the Rincón del Bonete reservoir and most of Uruguay's water bodies, with concentration peaks in February that remain until March or even April (González-Piana et al., 2017).

The results obtained for low and high Chl*a* schemes show that there is room for improvement before integrating satellite data products into operational WQ monitoring. Nevertheless, while numeric prediction accuracies can improve, a classification into discrete classes, such as trophic levels, can be helpful in reporting SDG 6. This could also be coupled with numeric transformations (not explored here), such as the Trophic State Index (TSI) (Carlson, 1977), which can help limit the range of outputs (Pahlevan et al., 2020). From a management perspective and for the SDG 6.3.2 reporting, the range-specific assessments become more relevant and provide a more reasonable alternative for evaluating the current state of practice. In that regard, MDN has consistently achieved high-quality results for binary classification, mainly for MSI and OLCI.

After the examination of the patterns shown in the E vs M scatterplots (Figures S3-S10), several schemes display promise: MDN with ACOLITE, Mishra NDCI, Gons (2 bands) & Drozd, with SeaDAS, for the MSI sensor, while MDN, Gons (2 bands) and Moses (3 bands), all with POLYMER, for OLCI. While some of these models have some tendency to produce outliers, such as Drozd, NDCI, or even MDN (with POLYMER), the range-specific classification results appear relevant to monitoring applications, as long as those extreme values deviate consistently in the correct direction and are skewed toward either tail of Chl*a* distribution.

5. Conclusions

Widespread water pollution induced primarily by anthropogenic pressure poses major threats to Uruguay's freshwater and coastal regions. One cause for water-quality impairments is HAB events that can be characterized and quantified via Chl*a*, the primary pig-

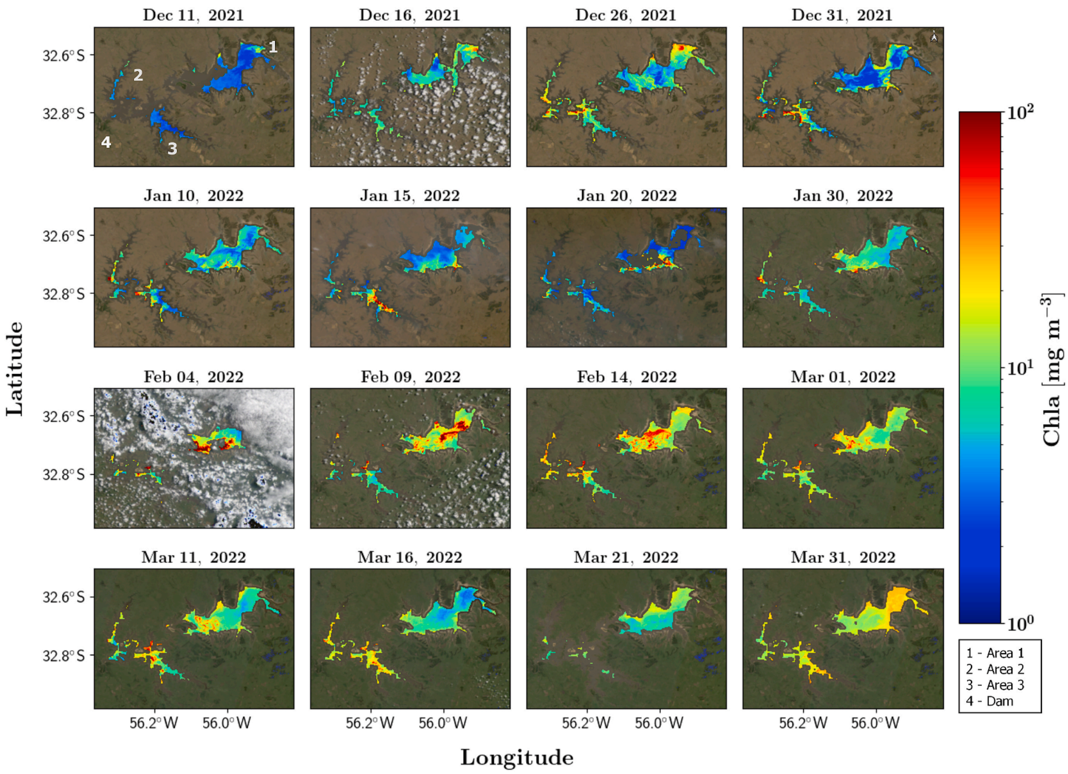

Fig. 8. Chl*a* maps produced for the Rincón del Bonete reservoir from MSI imagery processed via the MDN model and ACOLITE, from December 11th, 2021 to March 31st, 2022 (summer season). Due to adjacency effects from the surrounding clouds or nearby forested regions in narrow branches, pixels outside the water bodies (e.g. south-eastern dark patches, colored blue on March 21/2022) may be assigned with low Chl*a*, which should be ignored and/or flagged as low quality. The general direction of water flow is east-to-west, with the reservoir's dam located towards the westernmost side (Area 4).

ment in all phytoplankton types. This study offered a thorough appraisal of several image processing schemes to identify optimal Chl*a* products obtainable from optical satellite imagery that complement field-based monitoring exercises for effective and consistent assessment of water quality. Of three atmospheric correction (AC) processors and 17 state-of-the-art algorithms, using satellite matchups and two robust metrics (MNR and Youden's J statistic), we determined the most viable processing schemes in terms of overall accuracy and precision, as well as their ability to correctly classify waters into two discrete classes, defined by a threshold of 8 mg m^{-3} of Chl*a*). Our results show that the MDN model is often among the top performers, followed by Gons (2 bands) and Mishra NDCI algorithms. Regarding AC processors, our analysis suggests that, in general, POLYMER performs better for the OLCI sensor, SeaDAS can be a reasonable alternative when using OLI, and for MSI, there is no clear preference among the AC methods. We further demonstrated that the MDN model is the most reliable for correctly assigning pixels to the right Chl*a* range (i.e., Chl*a* $>$ or $<$ 8 mg m^{-3}), which can be a fundamentally key decision-making distinction for management and SDG 6.3.2 reporting on discriminating water bodies with good conditions.

Author contributions

J.M. Barreneche: Conceptualization, Methodology, Validation, Formal Analysis, Investigation, Data curation, Writing – Original Draft; B. Guigou: Conceptualization, Methodology, Investigation, Writing – Original Draft; F. Gallego: Conceptualization, Methodology, Investigation, Writing – Original Draft; A. Barbieri: Conceptualization, Methodology, Investigation; B. Smith: Methodology, Software, Validation, Data curation; M. Fernández: Conceptualization, Investigation; V. Fernández: Conceptualization, Project administration, Funding acquisition; N. Pahlevan: Conceptualization, Writing – Original Draft, Funding acquisition.

Ethical statement

The authors declare that all ethical practices have been followed in relation to the development, writing, and publication of the article.

Declaration of competing interest

The authors declare that they have no known competing financial interests or personal relationships that could have appeared to influence the work reported in this paper.

Data availability

A zip file is available with the data and code needed to reproduce all the analyses

Acknowledgements

We would like to thank the Ministry of Environment for providing free access to *in situ* data and the anonymous reviewers who offered helpful comments on an earlier draft of the manuscript. This work was funded by the Ministry of Environment of Uruguay and the National Aeronautics and Space Administration's (NASA) Applied Sciences in support of using and validating satellite image products for reporting and monitoring SDG 6.3.2.

Appendix A. Supplementary data

Supplementary data to this article can be found online at https://doi.org/10.1016/j.rsase.2022.100891.

References

Allard, M., World Health Organization, 1992. GEMS/WATER Operational Guide (No. GEMS/W. 92.1). World Health Organization.

Andries, A., Morse, S., Murphy, R., Lynch, J., Woolliams, E., Fonweban, J., 2019. Translation of Earth observation data into sustainable development indicators: an analytical framework. Sustain. Dev. 27, 366–376. https://doi.org/10.1002/sd.1908.

Aubriot, L., Delbene, L., Haakonsson, S., Somma, A., Hirsch, F., Bonilla, S., 2017. Evolución de la eutrofización en el Río Santa Lucía: influencia de la intensificación productiva y perspectivas. INNOTEC 14. https://doi.org/10.26461/14.04. 07–16. .

Balasubramanian, S.V., Pahlevan, N., Smith, B., Binding, C., Schalles, J., Loisel, H., Gurlin, D., Greb, S., Alikas, K., Randla, M., Bunkei, M., Moses, W., Nguyễn, H., Lehmann, M.K., O'Donnell, D., Ondrusek, M., Han, T.-H., Fichot, C.G., Moore, T., Boss, E., 2020. Robust algorithm for estimating total suspended solids (TSS) in inland and nearshore coastal waters. Rem. Sens. Environ. 246, 111768. https://doi.org/10.1016/j.rse.2020.111768.

Board, M.E.A., 2005. Ecosystems and Human Well-Being: Wetlands and Water Synthesis.

Bukata, R., Jerome, J., Kondratyev, K., Pozdnyakox, D., 1995. Optical Properties and Remote Sensing of Inland and Coastal Waters. CRC Press, New York. https://doi.org/10.1201/9780203744956.

Bulgarelli, B., Kiselev, V., Zibordi, G., 2014. Simulation and analysis of adjacency effects in coastal waters: a case study. Appl. Opt. 53, 1523–1545. https://doi.org/10.1201/9780203744956.

Carlson, R., 1977. A trophic state index for lakes. Limnology and oceanography. Limnol. Oceanogr. 22, 361–369. https://doi.org/10.4319/lo.1977.22.2.0361.

Cole, G., Weihe, P., 2015. Textbook of Limnology. Waveland Press.

Connor, R., 2015. The United Nations world water development report 2015: water for a sustainable world—UNESCO Biblioteca Digital. https://unesdoc.unesco.org/ark:/48223/pf0000231823.

de Ambiente, Ministerio, 2021. Observatorio Ambiental Nacional. https://www.ambiente.gub.uy/oan (Accessed 26 October 2022).

De Keukelaere, L., Sterckx, S., Adriaensen, S., Knaeps, E., Reusen, I., Giardino, C., Bresciani, M., Hunter, P.D., Neil, C., Van der Zande, D., Vaičiūtė, D., 2018. Atmospheric correction of Landsat-8/OLI and Sentinel-2/MSI data using iCOR algorithm: validation for coastal and inland waters. European Journal of Remote Sensing 51, 525–542. https://doi.org/10.1080/22797254.2018.1457937.

Drozd, A., de Tezanos Pinto, P., Fernández, V., Bazzalo, M., Bordet, F., Ibañez, G., 2020. Hyperspectral remote sensing monitoring of cyanobacteria blooms in a large South American reservoir: high- and medium-spatial resolution satellite algorithm simulation. Marine and Freshwater Research 71, 593–605. https://doi.org/10.1071/MF18429.

El Serafy, G., Schaeffer, B., Neely, M., Spinosa, A., Odermatt, D., Weathers, K., Baracchini, T., Bouffard, D., Carvalho, L., Conmy, R., Keukelaere, L., Hunter, P., Jamet, C., Joehnk, K., Johnston, J., Knudby, A., Minaudo, C., Pahlevan, N., Reusen, I., Rose, K., Schalles, J., Tzortziou, M., 2021. Integrating inland and coastal water quality data for actionable knowledge. Rem. Sens. 13, 2899. https://doi.org/10.3390/rs13152899.

Ferreira, B., Iten, M., Silva, R., 2020. Monitoring sustainable development by means of earth observation data and machine learning: a review. Environ. Sci. Eur. 32, 1–17. https://doi.org/10.1186/s12302-020-00397-4.

Gernez, P., Doxaran, D., Barillé, L., 2017. Shellfish aquaculture from space: potential of Sentinel2 to monitor tide-driven changes in turbidity, chlorophyll concentration and oyster physiological response at the scale of an oyster farm. Front. Mar. Sci. 4, 137. https://doi.org/10.3389/fmars.2017.00137.

Gilerson, A., Gitelson, A., Zhou, J., Gurlin, D., Moses, W., Ioannou, I., Ahmed, S., 2010. Algorithms for remote estimation of chlorophyll-a in coastal and inland waters using red and near infrared bands. Opt Express 18, 24109–24125. https://doi.org/10.1364/OE.18.024109.

Gitelson, A., 1992. The peak near 700 nm on radiance spectra of algae and water: relationships of its magnitude and position with chlorophyll concentration. Int. J. Rem. Sens. 13, 3367–3373. https://doi.org/10.1080/01431169208904125.

Gons, H.J., 1999. Optical teledetection of chlorophyll a in turbid inland waters. Environ. Sci. Technol. 33 (7), 1127–1132. https://doi.org/10.1021/es9809657.

González-Piana, M., Fabián, D., Piccardo, A., Chalar, G., 2017. Dynamics of total microcystin LR concentration in three subtropical hydroelectric generation reservoirs in Uruguay, south America. Bull. Environ. Contam. Toxicol. 99 (4), 488–492. https://doi.org/10.1007/s00128-017-2158-7.

Gordon, H., Clark, D., Brown, J., Brown, O., Evans, R., Broenkow, W., 1983. Phytoplankton pigment concentrations in the Middle Atlantic Bight: comparison of ship determinations and CZCS estimates. Appl. Opt. 22, 20–36. https://doi.org/10.1364/AO.22.000020.

Gorgoglione, A., Gregorio, J., Ríos, A., Alonso, J., Chreties, C., Fossati, M., 2020. Influence of land use/land cover on surface-water quality of santa lucía river, Uruguay. Sustainability 12 (11), 4692. https://doi.org/10.3390/su12114692.

Gurlin, D., Gitelson, A., Moses, W., 2011. Remote estimation of chl-a concentration in turbid productive waters — return to a simple two-band NIR-red model? Rem. Sens. Environ. 115 (12), 3479–3490. https://doi.org/10.1016/j.rse.2011.08.011.

Harmel, T., Chami, M., Tormos, T., Reynaud, N., Danis, P., 2018. Sunglint correction of the multi-spectral instrument (MSI)-SENTINEL-2 imagery over inland and sea waters from SWIR bands. Rem. Sens. Environ. 204, 308–321. https://doi.org/10.1016/J.RSE.2017.10.022.

Hurtado, S.I., 2020. RobustLinearReg: Robust Linear Regressions. The Comprehensive R Archive Network. https://CRAN.R-project.org/package=RobustLinearReg.

Maciel, F., Pedocchi, F., 2021. Evaluation of ACOLITE atmospheric correction methods for Landsat-8 and Sentinel-2 in the Río de la Plata turbid coastal waters. Int. J. Rem. Sens. 43, 215–240. https://doi.org/10.1080/01431161.2021.2009149.

Mélin, F., Zibordi, G., Berthon, J.-F., Bailey, S., Franz, B., Voss, K., Flora, S., Grant, M., 2011. Assessment of MERIS reflectance data as processed with SeaDAS over the European seas. Opt Express 19, 25657–25671. https://doi.org/10.1364/OE.19.025657.

Ministerio de Vivienda Ordenamiento Territorial y Medio Ambiente, 2017. Manual de procedimientos analíticos para muestras ambientales 2017. https://www.gub.uy/ministerio-ambiente/ (Accessed 26 October 2022).

Mishra, S., Mishra, D.R., 2012. Normalized difference chlorophyll index: a novel model for remote estimation of chlorophyll-a concentration in turbid productive waters. Rem. Sens. Environ. 117, 394–406. https://doi.org/10.1016/j.rse.2011.10.016.

Mograne, M.A., Jamet, C., Loisel, H., Vantrepotte, V., Mériaux, X., Cauvin, A., 2019. Evaluation of five atmospheric correction algorithms over French optically-complex waters for the sentinel-3A OLCI ocean color sensor. Rem. Sens. 11 (6), 668. https://doi.org/10.3390/rs11060668.

Morley, S., Brito, T., Welling, D., 2018. Measures of model performance based on the log accuracy ratio. Space Weather 16 (1), 69–88. https://doi.org/10.1002/2017SW001669.

Moses, W.J., Gitelson, A., Berdnikov, S., Povazhnyi, V., Moses, W., Gitelson, A., Povazhnyy, V., 2009. Estimation of chlorophyll-a concentration in case II waters using

MODIS and MERIS data—successes and challenges. Environ. Res. Lett. 4. https://doi.org/10.1088/1748-9326/4/4/045005.
Moses, W.J., Gitelson, A.A., Berdnikov, S., Saprygin, V., Povazhnyi, V., 2012. Operational MERIS-based NIR-red algorithms for estimating chlorophyll-a concentrations in coastal waters—the Azov Sea case study. Rem. Sens. Environ. 121, 118–124. https://doi.org/10.1016/j.rse.2012.01.024.
Moses, W.J., Sterckx, S., Montes, M.J., De Keukelaere, L., Knaeps, E., 2017. Atmospheric correction for inland waters. In: Bio-optical Modeling and Remote Sensing of Inland Waters. Elsevier, pp. 69–100. https://doi.org/10.1016/B978-0-12-804644-9.00003-3.
Neil, C., Spyrakos, E., Hunter, P., Tyler, A., 2019. A global approach for chlorophyll-a retrieval across optically complex inland waters based on optical water types. Rem. Sens. Environ. 229, 159–178. https://doi.org/10.1016/j.rse.2019.04.027.
Organization for Economic and Co-operative Development, 1982. Eutrophication of Waters: Monitoring, Assessment and Control. Paris, France, -10: 9264122982.
O', Reilly, J.E., Werdell, P.J., 2019. Chlorophyll algorithms for ocean color sensors-OC4, OC5 & OC6. Rem. Sens. Environ. 229, 32–47. https://doi.org/10.1016/j.rse.2019.04.021.
Pahlevan, N., Sarkar, S., Franz, B., Balasubramanian, S., He, J., 2017. Sentinel-2 MultiSpectral Instrument (MSI) data processing for aquatic science applications: demonstrations and validations. Rem. Sens. Environ. 201, 47–56. https://doi.org/10.1016/j.rse.2017.08.033.
Pahlevan, N., Chittimalli, S.K., Balasubramanian, S.V., Vellucci, V., 2019. Sentinel-2/Landsat-8 product consistency and implications for monitoring aquatic systems. Rem. Sens. Environ. 220, 19–29. https://doi.org/10.1016/j.rse.2018.10.027.
Pahlevan, N., Smith, B., Schalles, J., Binding, C., Cao, Z., Ma, R., Alikas, K., Kangro, K., Gurlin, D., Hà, N., Matsushita, B., Moses, W., Greb, S., Lehmann, M., Ondrusek, M., Oppelt, N., Stumpf, R., 2020. Seamless retrievals of chlorophyll-a from Sentinel-2 (MSI) and Sentinel-3 (OLCI) in inland and coastal waters: a machine-learning approach. Rem. Sens. Environ. 240 (111604). https://doi.org/10.1016/j.rse.2019.111604.
Pahlevan, N., Mangin, A., Balasubramanian, S., Smith, B., Alikas, K., Arai, K., Barbosa, C., Bélanger, S., Binding, C., Bresciani, M., Giardino, C., Gurlin, D., Fan, Y., Harmel, T., Hunter, P., Ishikaza, J., Kratzer, S., Lehmann, M., Ligi, M., Ma, R., Martin-Lauzer, F., Olmanson, L., Oppelt, N., Pan, Y., Peters, S., Reynaud, N., Sander de Carvalho, L., Simis, S., Spyrakos, E., Steinmetz, F., Stelzer, K., Sterckx, S., Tormos, T., Tyler, A., Vanhellemont, Q., Warren, M., 2021. ACIX-Aqua: a global assessment of atmospheric correction methods for Landsat-8 and Sentinel-2 over lakes, rivers, and coastal waters. Rem. Sens. Environ. 258, 112366. https://doi.org/10.1016/j.rse.2021.112366.
Palmer, S.C., Kutser, T., Hunter, P., 2015. Remote sensing of inland waters: challenges, progress and future directions. Rem. Sens. Environ. 157, 1–8. https://doi.org/10.1016/j.rse.2014.09.021.
Poddar, S., Chacko, N., Swain, D., 2019. Estimation of chlorophyll-a in northern coastal bay of bengal using landsat-8 OLI and sentinel-2 MSI sensors. Front. Mar. Sci. 6, 598. https://doi.org/10.3389/fmars.2019.00598.
R Core Team, 2018. R: A Language and Environment for Statistical Computing. R Foundation for Statistical Computing, Vienna, Austria. URL. https://www.R-project.org/.
Renosh, P.R., Doxaran, D., Keukelaere, L.D., Gossn, J.I., 2020. Evaluation of atmospheric correction algorithms for sentinel-2-MSI and sentinel-3-OLCI in highly turbid estuarine waters. Rem. Sens. 12, 1285. https://doi.org/10.3390/rs12081285.
Rodríguez-Gallego, L., Rodríguez-Graña, L., Conde, D., 2003. Las lagunas costeras de Uruguay: Estado actual del conocimiento. V Jornadas Nacionales de Ciencias del Mar, Mar del Plata, Argentina. https://www.dinama.gub.uy/oan/documentos/uploads/2016/12/Lagunas_costeras_Uruguay_conocimiento_actual_VJCM.pdf (Accessed 19 May 2022).
Smith, M., Robertson Lain, L., Bernard, S., 2018. An optimized Chlorophyll a switching algorithm for MERIS and OLCI in phytoplankton-dominated waters. Rem. Sens. Environ. 215, 217–227. https://doi.org/10.1016/j.rse.2018.06.002.
Steinmetz, F., Deschamps, P., &Ramon, R., 2011. Atmospheric correction in presence of sun glint: application to MERIS. Opt. Express 19, 9783–9800.
Vanhellemont, Q., 2019. Adaptation of the dark spectrum fitting atmospheric correction for aquatic applications of the Landsat and Sentinel-2 archives. Rem. Sens. Environ. 225, 175–192. https://doi.org/10.1016/j.rse.2019.03.010.
Warren, M.A., Simis, S.G.H., Martinez-Vicente, V., Poser, K., Bresciani, M., Alikas, K., Spyrakos, E., Giardino, C., Ansper, A., 2019. Assessment of atmospheric correction algorithms for the Sentinel-2A MultiSpectral Imager over coastal and inland waters. Rem. Sens. Environ. 225, 267–289. https://doi.org/10.1016/j.rse.2019.03.018.
Wetzel, R.G., 2001. Limnology: Lake and River Ecosystems. third ed. Academic Press, San Diego. ISBN 9780080574394.
World Health Organization, 2003. Guidelines for Safe Recreational Water Environments. Vol. 1: Coastal and Fresh Waters. World Health Organization, Geneva. https://apps.who.int/iris/handle/10665/42591 (Accessed 19 May 2022).
Yang, W., Matsushita, B., Chen, J., Fukushima, T., 2011. Estimating constituent concentrations in case II waters from MERIS satellite data by semi-analytical model optimizing and look-up tables. Rem. Sens. Environ. 115 (5), 1247–1259. https://doi.org/10.1016/j.rse.2011.01.007.
Youden, W., 1950. Index for rating diagnostic tests. Cancer 3 (1), 32–35. https://doi.org/10.1002/1097-0142(1950)3:1%3C32::AID-CNCR2820030106%3E3.0.CO;2-3.
Zabaleta, B., Achkar, M., Aubriot, L., 2021. Hotspot analysis of spatial distribution of algae blooms in small and medium water bodies. Environ. Monit. Assess. 193 (4), 221. https://doi.org/10.1007/s10661-021-08944-z.